Design and implementation of a nonlinear robust controller based on the disturbance observer for the active spray boom suspension

Longfei Cui, Xinyu Xue*, Wei Kong, Suming Ding, Wei Gu, Feixiang Le

(*Nanjing Institute for Agricultural Mechanization, Ministry of Agriculture and Rural Affairs, Nanjing 210014, China*)

Abstract: Spray boom vibrations are one of the main causes of the uneven distribution of agrochemicals. Using active suspension to maintain the correct height of nozzles is critical for obtaining a uniform spray pattern and minimizing the possibility of spray drift. However, the electro-hydraulic active pendulum boom suspension has nonlinear uncertain factors such as parameter uncertainties, external disturbances, model error, etc., which complicate the design of the controller. Therefore, this paper proposes a nonlinear robust feedback control method with disturbances compensation, which integrates a robust controller and disturbance observers through the backstepping method. Initially, to verify the performance of the controller, the Lyapunov stability theory is used to prove that the proposed controller can guarantee the given transient performance and the final tracking accuracy. Furthermore, taking the active suspension of a 28 m wide boom driven by a single-rod hydraulic actuator as an implementation case, the proposed NRCDC controller was compared with a variety of control schemes through a rapid control prototype of a pendulum active suspension. Finally, the proposed control scheme is implemented on a self-propelled sprayer with a boom of 12 m in length. The field test results show that all the performance indicators of the NRCDC controller are better than the other three conventional controllers. Both laboratory and field tests have verified the effectiveness and high performance of the proposed controller.

Keywords: robust control, sprayer boom, boom suspension, hydraulic control system, disturbance observer

DOI: 10.25165/j.ijabe.20231601.7007

Citation: Cui L F, Xue X Y, Kong W, Ding S M, Gu W, Le F X. Design and implementation of a nonlinear robust controller based on the disturbance observer for the active spray boom suspension. Int J Agric & Biol Eng, 2023; 16(1): 153–161.

1 Introduction

To increase the yield in agriculture, plants must be protected against diseases. One of the most important methods to spray agrochemicals is by using a spray boom. Agrochemicals are dissolved in a carrier liquid and sprayed using an agricultural spray boom. However, the uneven ground causes random vibration of the boom during operation, which deteriorates the deposition distribution pattern of the spray nozzle, resulting in overspray or missed spray of chemical pesticides[1-4], which has side effects on plants, heavy application of chemical pesticides has seriously polluted the environment[5-7]. The uniformity of application influences the amount of chemical or biological crop protection products delivered to individual plants, rows, or field areas. Studies point out that the rolling motion of the boom is responsible for variations in spray distribution ranging from 0 to 1000% (100% is ideal)[8-10]. Herbst et al.[11] presented methods for spray uniformity of booms under various field conditions and built a hydraulic test rig to simulate field conditions to test the effect of boom motion on spray deposits. Simulation results show that trailed booms have better spray distribution than tractor-mounted booms because trailed sprayers excite the boom with less intensity and their response frequency is reduced by 0.5 Hz for the 27 m boom. This paper focuses on the control of the rolling motion of the boom.

The boom suspension would be to maintain a constant distance between boom and ground to improve the uniformity with which the droplets are distributed through achieving correct overlap of spray patterns from adjacent nozzles. High efficiency can also be guaranteed by using longer booms or spraying at higher speeds by reducing vertical vibration at the boom tips. It should be possible to set the boom closer to the targets to enhance spray penetration through crop canopies and reduce the risk of spray drift[12,13]. Boom suspensions are generally classified as passive or active. A vast proportion of agricultural sprayers are equipped with a passive suspension[14]. Passive boom suspension maintains the system stiffness by reasonably selecting springs, dampers, and other linkages, which can better attenuate the high-frequency excitation from road roughness, but it cannot drive the boom to align the inclined ground[15]. Active boom suspension system has been adopted by many manufacturers of boom sprayers, but whether the active suspension systems can precisely control the angle of the boom depends on the design of high-performance controller[16,17].

This study proposes a nonlinear robust control method of an active pendulum boom suspension is proposed, an active boom suspension includes a set of the electro-hydraulic servo control system designed based on the original passive suspension, which consists of a hydraulic cylinder, two non-contact distance sensors and controller hardware, its design and calculation have been given in our previous research[18,19]. Driven by the hydraulic cylinder, the boom's roll angle tracks low-frequency terrain changes.

The common control methods, such as proportional control,

Received date: 2021-08-17 **Accepted date:** 2022-06-14

Biographies: Longfei Cui, PhD, Associate Research Fellow, research interest: dynamics and control of agricultural machinery, Email: cuilong.fei@163.com; **Wei Kong**, Associate Research Fellow, research interest: agricultural equipment and engineering; Email: iamkongwei@163.com; **Suming Ding**, Research Fellow, research interest: crop protection and mechanical engineering, Email: dsmchina@sina.com; **Wei Gu**, Associate Research Fellow, research interest: vibration control of spray boom, Email: 272430567@qq.com; **Feixiang Le**, Assistant Research Fellow, research interest: mechanical engineering, Email: 469579103@qq.com.

***Corresponding author: Xinyu Xue**, PhD, Research Fellow, research interest: crop protection and spraying machinery. Nanjing Research Institute for Agricultural Mechanization, Ministry of Agriculture and Rural Affairs, Nanjing 210014, China. Tel: +86-25-84346243, Email: xuexynj@qq.com.

LQG/LTR control, H_∞ control, and so on[20-22], whose control accuracy is mainly obtained by high gain feedback. If the gains are too large, the unmodeled dynamics of the boom suspension system will be easily excited. The electro-hydraulic servo system of suspension is a typical non-linear system that includes various parameter uncertainties and time-varying disturbances, which include unmatched disturbances (external disturbances, unmodeled dynamics, etc.) and matched disturbances (system pressure dynamic modeling error)[23]. The above factors will sharply degrade the expected control performance of the controller and make the design of high precision tracking controller becomes difficult. The adaptive robust control (ARC) strategy is proposed, which has been applied to a variety of controlled plants[24,25] and has good tracking performance, but its high tracking accuracy is achieved by using high feedback gains. An extended state observer (ESO) has been used to estimate the disturbance in the hydraulic system by Yao et al.[26,27], but this method cannot deal with both matched and mismatched disturbances. Active torque control scheme with iterative learning (ATCAIL) has been applied to the undesired vibration control of the boom[28,29], but due to the limitation of the output torque of the DC motor, it is not suitable for the motion control of a large boom with more than 27 m in length. An adaptive fuzzy sliding mode control strategy for the trapezoidal boom suspension was designed by Xue et al.[30], but this method does not explicitly process the parameter uncertainties, and its steady-state control performance is easily affected by factors such as changes in operating conditions and load quality.

To accurately estimate the strong uncertain nonlinearity in motion control, a finite time disturbance observer is designed[31], which can accurately estimate the uncertain nonlinearity of the system in a finite time and then carry out feedforward control. However, it needs to obtain the parameters of the system in advance[32-34].

Based on the above analysis, developing a high-precision controller for active pendulum boom suspension to deal with the parameter uncertainties and random disturbances of the suspension system may be a novel and valuable research hotspot. The mathematical model of the boom pendulum suspension electro-hydraulic position servo system is established. Aiming at the time-varying disturbances and parameter uncertainties existing in the electro-hydraulic suspension position servo system, a nonlinear robust feedback controller based on the finite time disturbance observers is designed, the finite time disturbance observers were integrated into the nonlinear robust feedback controller by using the backstepping design method, the disturbance observers are designed to observe the matched and mismatched disturbances simultaneously. All the parameter uncertainties in the model compensation control items are concentrated in the disturbance estimation items, combined with nonlinear robust feedback control, to complete the processing of disturbances and parameter uncertainties in the actual system. By using Lyapunov's theorem, it is proved that the proposed controller can guarantee the described instantaneous control accuracy and steady-state tracking error.

To verify the effectiveness of the proposed controller, an experimental study is carried out with a 28 m width boom active suspension driven by a single rod hydraulic actuator. The controller has been tested and verified through rapid prototyping control technology. The six-degree-of-freedom motion platform is used to simulate the field motion of the chassis. Finally, the proposed nonlinear robust controller for the active boom system is implemented on a self-propelled sprayer with a 12 m long boom, and the effectiveness of the boom control system was verified through experiments in paddy fields.

2 Problem formulation and dynamic models

2.1 Modeling of the pendulum boom suspension system

The schematic diagram of the active pendulum boom suspension is shown in Figure 1, where the boom is in any state during the control process. O is the rotation center of the pendulum rod, P is the rotation center of the boom, the length of the boom OP is l_1, the distance between the rotation shaft at point Q and the rotation shaft at point R is l_2, and the distance from the rotating shaft R to the welding point F on the spray boom is l_3, and the distance from rotating shaft P to welding point F on the boom is l_4. In the process of adjusting the boom angle by hydraulic cylinder, the angle between the rod PQ and rod PR is $\zeta_0+\zeta$.

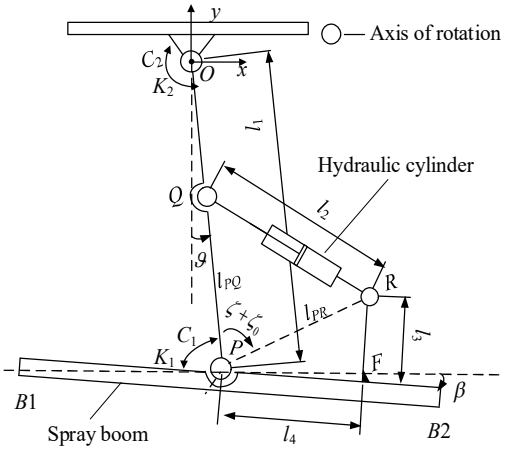

Figure 1 Simplified schematic diagram of active pendulum boom suspension

The linear motion of the hydraulic cylinder is transformed into the rolling motion of the spray bar through the designed connecting rod mechanism. Therefore, firstly, the kinematic and dynamic equations of the connecting rod mechanism are established. Then, the hydraulic system is designed and the model of the valve controlled hydraulic cylinder is established. According to the geometric relation of the linkage mechanism of active suspension and the cosine theorem, it can be obtained as,

$$\zeta = \arccos\frac{l_{PQ}^2 + l_{PR}^2 - l_2^2}{2l_{PQ}l_{PR}} - \zeta_0 \tag{1}$$

where, l_{PR} is the distance between point P and point R in Figure 1, m; l_{PQ} is the distance between point P and point Q, m; l_2 can be measured by the displacement sensor on the hydraulic cylinder, m.

The displacement of the piston rod of the hydraulic cylinder is $x_L=l_2-l_{20}$, then the speed of the piston of the hydraulic cylinder is

$$\dot{x}_L = \frac{l_{PQ}l_{PR}\sin(\zeta+\zeta_0)}{\sqrt{l_{PQ}^2 + l_{PR}^2 - 2l_{PQ}l_{PR}\cos(\zeta+\zeta_0)}}\dot{\zeta} \tag{2}$$

When the sprayer stops on horizontal ground, the pendulum OP is in the vertical position and the boom is in the horizontal position, define this state as the initial state of the boom suspension, in this condition $\vartheta=0$, $\beta=0$, the angle between rod PQ and rod PR is ζ_0, the length of the oil cylinder is l_{20}, and under the driving of the hydraulic cylinder, the angle variation between rod PQ and rod PR is ζ. The angle between boom and target position β can be obtained from suspension geometry:

$$\beta=\zeta+\vartheta \tag{3}$$

where, ϑ is the angle from which the pendulum rod OP deviates

from the initial position during the movement of the hydraulic cylinder, (°).

The control goal is to make the angle of the boom accurately track the desired trajectory, and realize the boom angle to follow the terrain fluctuation. The dynamic model can be described as follows

$$I_1\ddot{\beta}+K_1\beta+C_1\dot{\beta}+A_f S_f(\dot{\beta})+f(\beta,\dot{\beta},t)=g_1(A_1P_1-A_2P_2) \tag{4}$$

$$g_1=\frac{\partial x_L}{\partial\zeta}=\frac{l_{PQ}l_{PR}\sin(\zeta+\zeta_0)}{\sqrt{l_{PQ}{}^2+l_{PR}{}^2-2l_{PQ}l_{PR}\cos(\zeta+\zeta_0)}} \tag{5}$$

where, I_1 represents the moment of inertia of spray boom respectively, kg·m^2; K_1 is the suspension rotational stiffness coefficient around point O, N·m/rad; C_1 is the suspension rotational damping coefficient around point O, N·m·s/rad; A_f is the amplitude of approximate Coulomb friction, N·m; S_f is a continuous shape function, $f(\beta,\dot{\beta},t)$ represents the sum of unmodeled dynamics and external disturbances, including unmodeled nonlinear friction characteristics. A_1 and A_2 are the effective areas of the two chambers of the hydraulic cylinder, m^2; P_1 and P_2 are the oil pressure of the two chambers, Pa.

An asymmetrical servo valve is used to control the asymmetrical cylinder as the actuator of the boom active suspension. The schematic diagram is shown in Figure 2.

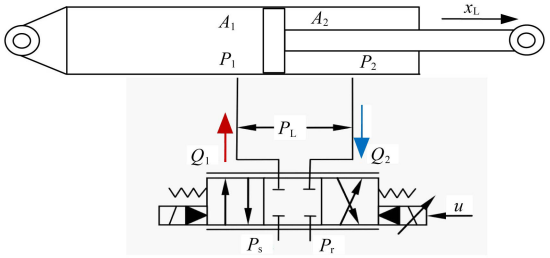

Figure 2 Schematic diagram of valve-controlled single rod hydraulic cylinder

The pressure dynamic equations of the forward chamber and return chamber are established as[35],

$$\dot{P}_1=\frac{\beta_{e1}}{V_1}(-A_1\dot{x}_L-C_tP_L+q_1+Q_1) \tag{6}$$

$$\dot{P}_2=\frac{\beta_{e2}}{V_2}(A_2\dot{x}_L-C_tP_L-q_2-Q_2) \tag{7}$$

where, $V_1=V_{01}+A_1x_L$, $V_2=V_{02}-A_2x_L$ represent the effective volumes of the forward chamber and return chamber, respectively; V_{01} and V_{02} are the initial volumes of the rod free chamber and the rod cavity respectively; Q_1 and Q_2 represent the flow from the servo valve to the two chambers of the hydraulic cylinder respectively; q_1 and q_2 are the lumped modeling errors in the dynamics of P_1 and P_2, m^3; β_{e1} and β_{e2} are the bulk moduli of the hydraulic oil in the left and right chambers of the hydraulic cylinder, Pa; C_t is the internal leakage coefficient, m^3/s·Pa; $P_L=P_1-P_2$ represents the load pressure, Pa; the flow Q_1, Q_2 of servo valve is a function of spool displacement x_v, m^3/s; and the flow equation can be expressed as follows[35]:

$$\begin{cases}Q_1=\sqrt{2}k_{q1}k_iR_1u\\ Q_2=\sqrt{2}k_{q2}k_iR_2u\end{cases} \tag{8}$$

where, k_i and u represent the current gain of spool and control input respectively, and the expressions of R_1 and R_2 are as follows:

$$\begin{cases}R_1=s(u)\sqrt{P_s-P_1}+s(-u)\sqrt{P_1-P_r}\\ R_2=s(u)\sqrt{P_2-P_r}+s(-u)\sqrt{P_s-P_2}\end{cases} \tag{9}$$

$s(*)$ is defined as follows:

$$s(*)=\begin{cases}1 & \text{if } *\geq 0\\ 0 & \text{if } *<0\end{cases} \tag{10}$$

where, P_s and P_r are the supply pressure and return pressure; k_{q1} and k_{q2} are the flow gain coefficient of the left and right cavities.

$$\begin{cases}k_{q1}=C_dw_1\sqrt{\dfrac{1}{\rho}}\\ k_{q2}=C_dw_2\sqrt{\dfrac{1}{\rho}}\end{cases} \tag{11}$$

where, C_d is the flow coefficient of servo valve orifice, w_1 and w_2 are the area gradient of left and right ends of servo valve spool orifice, m^2, ρ is the density of hydraulic oil, kg/m^3. Since the servo valve is symmetrical, the flow gain coefficient $k_{q1}=k_{q2}=k_q$, and the elastic modulus of the two-cavity hydraulic oil of the actuator satisfies $\beta_{e1}=\beta_{e2}=\beta_e$.

3 Design of nonlinear robust controller based on disturbance compensation

3.1 The state equation of electro-hydraulic suspension

Define state variables $\boldsymbol{x}=[x_1,\ x_2,\ x_3]^T=[\beta,\dot{\beta},(A_1P_1-A_2P_2)/I_1]^T$, then the dynamic model can be written in the form of state space as follows

$$\begin{cases}\dot{x}_1=x_2\\ \dot{x}_2=g_1x_3-\dfrac{C_1}{I_1}x_2-\dfrac{K_1}{I_1}x_1-\dfrac{A_f}{I_1}S_f(x_2)-d_1(x,t)\\ \dot{x}_3=\dfrac{\beta_ek_u}{I_1}f_{31}u-\dfrac{\beta_e}{I_1}f_{32}-\dfrac{\beta_eC_t}{I_1}f_{33}-d_2(x,t)\end{cases} \tag{12}$$

where,

$$\begin{cases}f_{31}=\dfrac{A_1}{V_1}R_1+\dfrac{A_2}{V_2}R_2\\ f_{32}=(\dfrac{A_1^2}{V_1}+\dfrac{A_2^2}{V_2})g_1x_2\\ f_{33}=(\dfrac{A_1}{V_1}+\dfrac{A_2}{V_2})P_L\\ d_1(\boldsymbol{x},t)=\dfrac{f(x,t)}{I_1}\\ d_2(\boldsymbol{x},t)=\dfrac{\beta_e}{I_1}(\dfrac{A_1}{V_1}q_1+\dfrac{A_2}{V_2}q_2)\end{cases} \tag{13}$$

The parameter set is defined as$\boldsymbol{\theta}=[\theta_1,\theta_2,\theta_3,\theta_4,\theta_5,\theta_6]^T$, where $\theta_1=K_1/I_1$, $\theta_2=C_1/I_1$, $\theta_3=A_f/I_1$, $\theta_4=\beta_e\cdot k_u/I_1$, $\theta_5=\beta_e/I_1$, $\theta_6=\beta_e\cdot C_t/I_1$. The state-space equation of boom suspension can be formulated as

$$\begin{cases}\dot{x}_1=x_2\\ \dot{x}_2=g_1x_3-\theta_1x_1-\theta_2x_2-\theta_3S_f(x_2)-d_1(\boldsymbol{x},t)\\ \dot{x}_3=\theta_4f_{31}u-\theta_5f_{32}-\theta_6f_{33}-d_2(\boldsymbol{x},t)\end{cases} \tag{14}$$

The uncertain nonlinear terms d_1 and d_2 in the actual hydraulic system are bounded. So, the following assumptions are true

Hypothesis 1: $d_1(\boldsymbol{x},t)$, $\dot{d}_1(\boldsymbol{x},t)$ and $d_2(\boldsymbol{x},t)$ are all bounded, that is

$$\begin{cases}|d_1(\boldsymbol{x},t)|\leq\zeta_1\\ |\dot{d}_1(\boldsymbol{x},t)|\leq\zeta_2\\ |d_2(\boldsymbol{x},t)|\leq\zeta_3\end{cases} \tag{15}$$

where, ζ_1, ζ_2 and ζ_3 are positive bounded functions.

Hypothesis 2: the system reference command signal $x_{1d}(t)$ is third-order continuous, and the system expected position command, speed command, acceleration command, and acceleration

command are all bounded.

Let θ_{in} be the nominal value of θ_i and $\tilde{\theta}_i$ the estimation error of θ_i, and $\tilde{\theta}_i = \theta_{in} - \theta_i$, then the state equations are as follows

$$\begin{cases} \dot{x}_1 = x_2 \\ \dot{x}_2 = g_1 x_3 - \theta_{1n} x_1 - \theta_{2n} x_2 - \theta_{3n} S_{\mathrm{f}}(x_2) - D_1(\boldsymbol{x}, t) \\ \dot{x}_3 = \theta_{4n} f_{31} u - \theta_{5n} f_{32} - \theta_{6n} f_{33} - D_2(\boldsymbol{x}, t) \end{cases} \tag{16}$$

where,

$$\begin{cases} D_1(x,t) = \tilde{\theta}_1 x_1 + \tilde{\theta}_2 x_2 + \tilde{\theta}_3 S_{\mathrm{f}}(x_2) - d_1(x,t) \\ D_2(x,t) = -\tilde{\theta}_4 f_{31} u + \tilde{\theta}_5 f_{32} + \tilde{\theta}_6 f_{33} - d_2(x,t) \end{cases} \tag{17}$$

where, $D_1(x, t)$ is the mismatched concentrated disturbance, and $D_2(x, t)$ is the matched concentrated disturbance. To compensate for the mismatched and matched disturbances in the active suspension system simultaneously in one controller, the disturbance observers are designed as follows

$$\begin{aligned} &\dot{\hat{x}}_2 = \omega_0 + g_1 x_3 - \hat{\theta}_1 x_1 - \hat{\theta}_2 x_2 - \hat{\theta}_3 S_{\mathrm{f}}(x_2), \omega_1 = \dot{\hat{D}}_1, \omega_2 = \dot{\hat{D}}_1 \\ &\omega_0 = -a_1 \left| \hat{x}_2 - x_2 \right|^{2/3} \mathrm{sign}(\hat{x}_2 - x_2) + \hat{D}_1 \\ &\omega_1 = -a_2 \left| \hat{D}_1 - \omega_0 \right|^{1/2} \mathrm{sign}(\hat{D}_1 - \omega_0) + \hat{D}_1 \\ &\omega_2 = -a_3 \mathrm{sign}(\hat{D}_1 - \omega_1) \\ &\dot{\hat{x}}_3 = \omega_3 + \hat{\theta}_4 f_{31} u - \hat{\theta}_5 f_{32} - \hat{\theta}_6 f_{33}, \omega_4 = \dot{\hat{D}}_2 \\ &\omega_3 = -a_4 \left| \hat{x}_3 - x_3 \right|^{1/2} \mathrm{sign}(\hat{x}_3 - x_3) + \hat{D}_2 \\ &\omega_4 = -a_5 \mathrm{sign}(\hat{D}_2 - \omega_3) \end{aligned} \tag{18}$$

where, a_i>0 (i=1,2,3,4,5) is the coefficient of the observer, and μ_0, μ_3, μ_1, μ_2, μ_4 are the estimated values of x_2, x_3, D_1, $\dot{D}_1$, D_2, respectively. The estimation errors are defined as $\sigma_0=\mu_0-x_2$, $\sigma_1=\mu_1-D_1$, $\sigma_2=\mu_2-\dot{D}_1$, $\sigma_3=\mu_3-x_3$, $\sigma_4=\mu_4-D_2$, according to Equations (16) and (18), the dynamic observation errors of the observers can be deduced that

$$\begin{aligned} &\dot{\sigma}_0 = -a_1 \left| \sigma_0 \right|^{2/3} \mathrm{sign}(\sigma_0) + \sigma_1 \\ &\dot{\sigma}_1 = -a_2 \left| \sigma_1 - \dot{\sigma}_0 \right|^{1/2} \mathrm{sign}(\sigma_1 - \dot{\sigma}_0) + \sigma_2 \\ &\dot{\sigma}_2 \in -a_3 \mathrm{sign}(\sigma_2 - \dot{\sigma}_1) + \left[-L_1, L_1 \right] \\ &\dot{\sigma}_3 = -a_4 \left| \sigma_4 \right|^{1/2} \mathrm{sign}(\sigma_3) + \sigma_4 \\ &\dot{\sigma}_4 \in -a_5 \mathrm{sign}(\sigma_4 - \dot{\sigma}_3) + \left[-L_2, L_2 \right] \end{aligned} \tag{19}$$

where, L_k is the Lipschitz constant of $D_k^{(3-k)}$ (k =1,2). The theoretical analysis in reference [36] shows that the observer can guarantee global finite-time stability, that is, there is a finite time t_0 such that the dynamic observation error σ_i=0.

3.2 Controller design

The backstepping design method[37] is used to design the controller. The error variables are defined as follows

$$z_1 = x_1 - x_{1\mathrm{d}} \tag{20}$$

$$z_2 = \dot{z}_1 + k_1 z_1 = x_2 - x_{2eq},\ x_{2eq} = x_{1\mathrm{d}} - k_1 z_1 \tag{21}$$

where, z_1 represents the tracking error of the system, and k_1 is the positive feedback gain. Since $z_1(\mathrm{s}) = G(\mathrm{s})\, z_2(\mathrm{s})$, $G(\mathrm{s})=1/(\mathrm{s}+k_1)$ is a stable transfer function, it can be seen from the linear system theory that when z_2 tends to 0, z_1 also tend to 0. From (16) and (21), the derivative of z_2 with respect to time is as follows

$$\begin{aligned} \dot{z}_2 &= \dot{x}_2 - \dot{x}_{2eq} \\ &= g_1 x_3 - \theta_{1n} x_1 - \theta_{2n} x_2 - \theta_{3n} S_{\mathrm{f}}(x_2) + D_1(x,t) - \dot{x}_{2eq} \end{aligned} \tag{22}$$

Based on the disturbance estimations observed by the disturbance observers, the virtual control law α_2 can be designed as follows

$$\begin{cases} \alpha_2 = \dfrac{1}{g_1}(\alpha_{2a} + \alpha_{2s}) \\ \alpha_{2a} = \dot{x}_{2eq} + \theta_{1n} x_1 + \theta_{2n} x_2 + \theta_{3n} S_{\mathrm{f}}(x_2) - \hat{D}_1 \\ \alpha_{2s} = -k_2 z_2 \end{cases} \tag{23}$$

where, α_{2a} is the model compensation term; α_{2s} is the linear feedback term, and k_2 is the set positive nonlinear gain. The deviation between control function α_2 and virtual control input x_3 is defined as $z_3=x_3-\alpha_2$, and by substituting Equation (23) into (22), one obtains

$$\begin{aligned} \dot{z}_2 &= g_1(z_3 + \alpha_2) - \theta_{1n} x_1 - \theta_{2n} x_2 - \theta_{3n} S_{\mathrm{f}}(x_2) + D_1(x,t) - \dot{x}_{2eq} \\ &= g_1 z_3 - \tilde{D}_1 - k_2 z_2 \end{aligned} \tag{24}$$

where the estimation error $\tilde{D}_1 = \tilde{D}_1 - D_1$.

Combined with Equation (16), the derivative of z_3 can be obtained

$$\begin{aligned} \dot{z}_3 &= \dot{x}_3 - \dot{\alpha}_2 \\ &= \theta_{4n} f_{31} u - \theta_{5n} f_{32} - \theta_{6n} f_{33} + D_2(x,t) - \dot{\alpha}_2 \end{aligned} \tag{25}$$

where,

$$\begin{cases} \dot{\alpha}_2 = \dot{\alpha}_{2\mathrm{c}} + \dot{\alpha}_{2\mathrm{u}} \\ \dot{\alpha}_{2c} = \dfrac{\partial \alpha_2}{\partial t} + \dfrac{\partial \alpha_2}{\partial x_1} x_2 + \dfrac{\partial \alpha_2}{\partial x_2} \dot{\hat{x}}_2 + \dfrac{\partial \alpha_2}{\partial \hat{D}_1} \dot{\hat{D}}_1 \\ \dot{\alpha}_{2u} = \dfrac{\partial \alpha_2}{\partial x_2} \tilde{\dot{x}}_2 = \left[\theta_{1n} + \theta_{3n} \dot{S}_{\mathrm{f}}(x_2) - k_1 - k_2 \right] \tilde{D}_1 \end{cases} \tag{26}$$

where, $\dot{\alpha}_{2\mathrm{c}}$ is the calculable partial differential part and $\dot{\alpha}_{2\mathrm{u}}$ is the incalculable part.

Based on Equations (24) and (26), the feedback nonlinear robust controller u is proposed as follows

$$\begin{cases} u = (u_a + u_s) / \theta_{4n} f_{31} \\ u_a = \theta_{5n} f_{32} + \theta_{6n} f_{33} - \hat{D}_2(x,t) + \dot{\alpha}_{2c} \\ u_s = -k_3 z_3 \end{cases} \tag{27}$$

where k_3>0 is the controller design parameter, u_{a} is the model compensation term, and u_{s} is the robust feedback term. Substituting Equation (27) into (25), the dynamic equation of z_3 can be obtained that

$$\dot{z}_3 = -\tilde{D}_2 - k_3 z_3 - [\theta_{1n} + \theta_{3n} \dot{S}_{\mathrm{f}}(x2) - k_1 - k_2] \tilde{D}_1 \tag{28}$$

3.3 Performance analysis of controller

Theorem: Since $d_1(\boldsymbol{x}, t)$ and $d_2(\boldsymbol{x}, t)$ are bounded, the appropriate feedback parameters k_1, k_2, and k_3 are selected to ensure that the matrix $\boldsymbol{\Lambda}$ defined below is a positive definite matrix

$$\boldsymbol{\Lambda} = \begin{bmatrix} k_1 & -\dfrac{1}{2} & 0 \\ -\dfrac{1}{2} & k_2 - \dfrac{1}{2} & -\dfrac{g_1}{2} \\ 0 & -\dfrac{g_1}{2} & \dfrac{1}{2}(2k_3 - \left| k_1 + k_2 - \theta_{1n} - \theta_{3n} \dot{S}_{\mathrm{f\,min}} \right| - 1) \end{bmatrix} \tag{29}$$

Then the designed controller (27) has the following conclusions:

(a) In actual engineering, the measured signals are all bounded. In addition, define the Lyapunov function as

$$V = \frac{1}{2} z_1^2 + \frac{1}{2} z_2^2 + \frac{1}{2} z_3^2 \tag{30}$$

Then, V satisfies the following inequality

$$V \le e^{-\mu t} V(0) + \frac{\varepsilon}{\mu} \left[1 - e^{-\mu t} \right] \tag{31}$$

where, $\mu=2\lambda_{\min}(\boldsymbol{\Lambda})$, $\lambda_{\min}(\boldsymbol{\Lambda})$ is the smallest eigenvalue of the positive definite matrix $\boldsymbol{\Lambda}$, and ε is a non-negative coefficient.

(b) After a finite time t_0, the system can obtain the accurate disturbance estimations through the designed disturbance observers, that is, $\tilde{D}_1=0$, $\dot{\tilde{D}}_1=0$, $\tilde{D}_2=0$.

In addition to the conclusion (a), the proposed controller can also guarantee the asymptotic tracking performance of the electro-hydraulic servo system, that is, when the time tends to infinity, the system error z can gradually converge to 0, that is, when $t\to\infty$, $z\to 0$, where $z=[z_1, z_2, z_3]^{\mathrm{T}}$.

Proof of Theorem. Based on Equations (20)-(22), and (28), the time derivative of V is

$$\begin{aligned}\dot{V} &= z_1\dot{z}_1 + z_2\dot{z}_2 + z_3\dot{z}_3 \\ &= z_1(z_2 - k_1z_1) + z_2(g_1z_3 - \tilde{D}_1 - k_2z_z) \\ &\quad + z_3[-\tilde{D}_2 - k_3z_3 - (\theta_{3n}\dot{S}_{\mathrm{f}} + \theta_{1n} - k_1 - k_2)\tilde{D}_1] \\ &\le -k_1z_1^2 + z_1z_2 - k_2z_2^2 + g_1z_2z_3 - z_2\tilde{D}_1 - k_3z_3^2 \\ &\quad - \tilde{D}_2z_3 + \left[k_1 + k_2 - \theta_{1n} - \theta_{3n}\dot{S}_{\mathrm{f\,min}}\right]\tilde{D}_1z_3 \\ &\le -[k_1z_1^2 - z_1z_2 + (k_2 - \frac{1}{2})z_2^2 - g_1z_2z_3 \\ &\quad + \frac{1}{2}(-1 + 2k_3 - \left|k_1 + k_2 - \theta_{1n} - \theta_{3n}\dot{S}_{\mathrm{f\,min}}\right|)z_3^2] \\ &\quad + \frac{1}{2}\tilde{D}_1^2 + \frac{1}{2}\left|k_1 + k_2 - \theta_{1n} - \theta_{3n}\dot{S}_{\mathrm{f\,min}}\right|\tilde{D}_1^2\end{aligned} \tag{32}$$

The feedback gains k_1, k_2, and k_3 are designed to ensure that the matrix $\boldsymbol{\Lambda}$ becomes a positive definite matrix

$$\dot{V} \le -2\lambda_{\min}(\boldsymbol{\Lambda})V + \varepsilon \le -\mu V + \varepsilon \tag{33}$$

where, $\mu=2\lambda_{\min}(\boldsymbol{\Lambda})$, $\lambda_{\min}(\boldsymbol{\Lambda})$ is the minimum eigenvalue of positive definite matrix, and

$$\varepsilon = \frac{1}{2}\tilde{D}_1^2 + \frac{1}{2}\left|k_1 + k_2 - \theta_{1n} - \theta_{3n}\dot{S}_{\mathrm{f\,min}}\right|\tilde{D}_1^2 \tag{34}$$

After performing the integral transformation at both ends of Equation (33), we can get

$$V \le e^{-\mu t}V(0) + \frac{\varepsilon}{\mu}[1 - e^{-\mu t}] \tag{35}$$

Therefore, it is proved that the Lyapunov function V is globally bounded, assuming that the given motion trajectory is bounded, it can be seen from Equation (16) that the system output signal is bounded, that is, z_1, z_2, and z_3 are bounded, and from Equation (27), it can be seen that the control command u is also bounded. The conclusion (a) is proved.

The following is proof of conclusion (b). When $t>t_0$, $\tilde{D}_1=0$, $\dot{\tilde{D}}_1=0$, $\tilde{D}_2=0$, then the derivation of the Lyapunov equation is

$$\begin{aligned}\dot{V} &= z_1\dot{z}_1 + z_2\dot{z}_2 + z_3\dot{z}_3 \\ &= -k_1z_1^2 + z_1z_2 - k_2z_2^2 + g_1z_2z_3 - k_3z_3^2 \\ &\le -2\lambda_{\min}(\boldsymbol{\Lambda}_1)V = -W\end{aligned} \tag{36}$$

where,

$$\boldsymbol{\Lambda}_1 = \begin{bmatrix} k_1 & -\frac{1}{2} & 0 \\ -\frac{1}{2} & k_2 & -\frac{g_1}{2} \\ 0 & -\frac{g_1}{2} & k_3 \end{bmatrix} \tag{37}$$

Since W is always non-negative, $W\in L_2$, and $\dot{W}\in L\infty$, W is uniformly continuous. Based on the Barbalet lemma[38], when $t\to\infty$, $W\to 0$ implies conclusion (b). From the above analysis, it can be seen that the designed disturbance observers can process matched interference and unmatched interference at the same time, and can reach a bounded and stable state. In a limited time, the disturbance observers can accurately estimate the disturbance and eliminate the influence of the disturbance.

4 Comparative experiments

4.1 Experiment setup

To verify the effectiveness of the nonlinear robust feedback control strategy based on disturbance compensation, an active electro-hydraulic boom suspension experimental platform as shown in Figure 3 is established. The platform is mainly composed of a six-degree-of-freedom motion simulator, a boom, its pendulum suspension, a hydraulic position system, a hydraulic station, and a set of real-time measurement and control systems. The structural parameters of pendulum suspension are listed in Table 1.

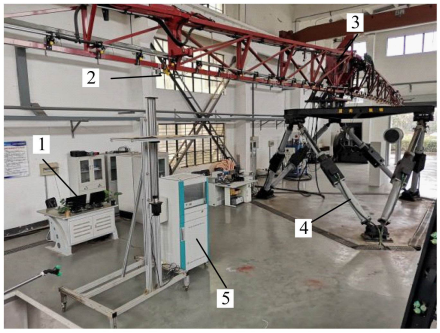

1. Console 2. Contactless ranging sensors 3. spray boom with pendulum active suspension 4. Six-degree-of-freedom motion simulation platform 5. Measurement and control system.

Figure 3 Experimental platform of the active electro-hydraulic boom suspension

Table 1 Structural parameters of boom suspension

Symbol	Parameters	Value
M_1	Total mass of boom/kg	970.6
I_1	Moment of inertia of boom/kg·m^2	32700
l_1	Length of pendulum rod OP/m	0.980
l_{PR}	The distance between the shaft P and the shaft R /m	0.570
l_{PQ}	The distance between the shaft P and the shaft Q /m	0.615
l_{20}	Length of hydraulic cylinder in the initial state /m	0.460

In this study, the designed control algorithm was verified by using the rapid control prototype technology. Specific implementation steps: first, use the control algorithm development software (Simulink, MathWorks Inc, Massachusetts, USA) to conduct offline simulation of the controller, confirm the logic correctness, and convert it into C code for compilation; Second, the compiled control algorithm was imported into the real-time test and simulation software (VeriStand, National Instruments, Texas, USA), and the input and output signals in the control algorithm are mapped to the channels on a multi-function I/O board (PXIE 6358, National Instrument, Texas, USA). It enables the communication between the controller running on the National Instruments PXI embedded real-time processor and the sensors and hydraulic valves on the active suspension system. Moreover, monitoring software was developed with Veristand, which associates virtual instrument controls to model parameters or hardware channels to realize real-time monitoring and online interaction. During the test, we need to start the control system, observe the movement of the boom, and record the test data, the motion of the six-degree-of-freedom motion simulation platform is used to simulate the disturbance excitation of the sprayer chassis.

The electro-hydraulic servo system of the pendulum suspension includes a single-rod asymmetric hydraulic cylinder,

whose inner diameter is 22 mm, piston diameter is 40 mm, the effective stroke is 180 mm, and two contactless ranging sensors mounted on the tip of the boom (LTF12UC2LDQ, Bonner, Minnesota, USA), with an accuracy of ±1 mm, used to measure the distance between the two ends of the boom and the target, a magneto strictive displacement sensor (RHM0200MD60, MTS, Minnesota, USA) for measuring the position of the hydraulic cylinder, with an accuracy of ±2.5 μm, an inertial measurement sensor (Ellipse-D-G4A2-B1, SBG, France) for measuring the swing angle of the bar *OP*, with a dynamic measurement accuracy of 0.05°, two pressure sensors for measuring the pressure of the left and right chambers of the hydraulic cylinder (US5300-200BG, MEAS, Texas, USA), with an accuracy of 0.2 MPa, a servo valve (G761-3003, Moog, New York, USA) that controls the motion of the hydraulic cylinder, and 1 set of measurement and control system hardware systems (PXIe-1078, National Instruments, Texas, USA), whose function is to collect various sensor signals and output control commands to the servo valve.

4.2 Comparative experimental results

To verify the effectiveness of the designed control strategy, the proposed non-linear robust controller with disturbance compensation (NRCDC) is compared with the other three conventional controllers. The differences between the four controllers are as follows:

NRCDC controller integrates disturbance observers based on nonlinear robust control based on model compensation. Compared with the NRCDC controller proposed in this paper, the FLC controller lacks the interference compensation term, the RFC controller lacks model compensation and interference compensation terms, and VFPI is a proportional-integral controller with velocity feedforward, that is, based on the traditional PI controller, a velocity feedforward term is added. This control method is used by conventional spray bar controllers.

The introduction of each control strategy and the parameter values are as follows

1) **NRCDC**: This is the proposed NRCDC controller designed for the pendulum active suspension system, the oil source pressure Ps=10 MPa, and the oil return pressure Pr=0.08 MPa during the test. The total flow gain of the system k_t=k_t=1.21×10^{-8} m^3/(sV·$\sqrt{\text{Pa}}$). Choose the shape function of the frictional force as $S_f(x_2)$ = π·arctan(900x_2)/2. The controller feedback gains are given by k_1=100, k_2=4, k_3=2. The nominal values of unknown parameters in the suspension system are obtained by direct measurement or experimental identification, [θ_{1n}, θ_{2n}, θ_{3n}, θ_{4n}, θ_{5n}, θ_{6n}]^T = [22.26, 12.13, 0.22, 8.6×10^{-3}, 2.159×10^5, 2.159×10^{-7}, 1.1×10^{-10}]^T, the parameters of the disturbance observers are given by a_1=1000, a_2=200, a_3=150, a_4=1000, a_5=120.

2) **FLC***:* This is a feedback linearization controller commonly used in the hydraulic control system. It is obtained by using the same control law as in NRCDC. The difference between FLC and NRCDC is that the FLC controller does not use the disturbance compensation, and the gains of the FLC controller are k_1=100, k_2=4, k_3=2.

3) **RFC**: This is a direct robust feedback controller. Compared with the control law of NRCDC, RFC only contains the robust feedback part of NRCDC, it has no model compensation and disturbance estimation, and also adopts the same feedback gains as the NRCDC controller.

4) **VFPI***:* This is the velocity feed-forward proportional-integral controller. The controller gain is adjusted by the experiment and error method, its proportional coefficient k_p=140, integral coefficient k_i=31.20, and feedforward coefficient k_f=2.10.

The above control parameters are determined by repeated tests, and increasing the parameters based on the determined control parameters will introduce a lot of measurement noise or excite the high-frequency dynamics of the boom suspension system, thus making the system unstable. Therefore, the comparative experiment of the four controllers is reasonable. To quantify the performance of the above four controllers, the maximum absolute value of the tracking error M_e, the average value of tracking error μ, and the standard deviation of tracking error σ are used as evaluation indexes, and their definitions were given in Yao et al.[26]

To test the tracking performance of the designed controller, the target trajectory of the boom is set as x_{1d} = 0.05sin(t) rad. Input the amplitude and frequency of the target trajectory through the user interface, and then start the real-time control system and record all the state parameters during the algorithm execution. The control error is shown in Figure 4a. In the beginning, the boom tracking error is 0.62°. With the increase in experiment time, the measured trajectory of the boom tends to be consistent with the target trajectory, and the control system enters into a steady state. The maximum absolute error in time is 0.084°, which proves that the designed NRCDC control algorithm has progressive tracking.

The trajectories of β, ζ, and ϑ are shown in Figure 4. ϑ is the offset angle of pendulum rod *OP* under the action of chassis shaking disturbance and reaction force of hydraulic cylinder, which belongs to the uncertain disturbance in the control system. In the case of uncertain disturbance, the designed NRCDC controller can still reduce the error in a small range, ensuring the steady-state tracking accuracy of the boom.

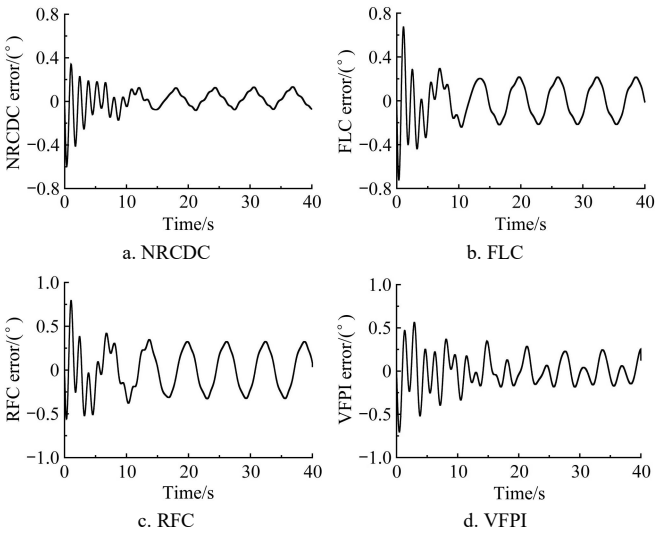

Figure 4 Tracking errors of 4 controllers in the comparison experiment

The other three control methods are tested in turn by using the large boom electro-hydraulic active suspension experimental platform. The tracking error comparison is shown in Figure 4. After the control system enters the steady state, taking three cycles of tracking error data to calculate the performance index of the controller, as listed in Table 2.

Due to the effect of disturbance compensation and model compensation, the proposed controller achieves the best control performance, and its steady-state control error is 0.134°.

Compared with the tracking error of the NRCDC controller and FLC controller (Figures 4a and 4b), the maximum absolute error of the FLC controller is 0.219°. Since the FLC controller

cannot handle the uncertainty disturbance and parameter uncertainties of the suspension system, the control accuracy depends on the model compensation control law and the nominal value robust control law, so under the same feedback gain, the performance index of the FLC controller It is worse than the NRCDC controller. The comparison experiment shows that the disturbance observers used in this paper can improve the control accuracy of the system.

Table 2 Performance indexes in the last three cycles after the system enters the stable state

Indexes	M_e/(°)	μ/(°)	σ/(°)
NRCDC	0.134	0.573	0.036
FLC	0.219	0.138	0.061
RFC	0.328	0.211	0.091
VFPI	0.286	0.108	0.072

Note: M_e, μ, and σ represent the maximum, average, and standard deviation of the absolute value of the error, respectively.

Comparing the tracking error of the RFC controller and the VFPI controller (Figure 4c and Figure 4d), the maximum absolute error of the RFC controller is 0.328° and that of the VFPI controller is 0.286°. The performance indicators of RFC and VFPI controllers are greater than those of the other two controllers. This is because these two controllers do not use model compensation and disturbance compensation, and only have certain robustness to the uncertainty of the electro-hydraulic suspension system. The advantages of designing the controller based on the pendulum nonlinear model are proved.

The performance indicators of RFC are worse than that of VFPI, mainly due to the use of feedback gains k_1, k_2, and k_3 in RFC, NRCDC, and FLC, which are smaller than the gains in the VFPI controller. Nevertheless, under the effect of the model compensation control law, the tracking error of the NRCDC controller and the FLC controller is smaller than that of the VFPI controller. This shows that the NRCDC controller can achieve better tracking performance with smaller feedback gains, which can avoid the problem of boom resonance caused by high-gain feedback.

The disturbance estimation of NRCDC is shown in Figure 5. As the experiment time increases, the disturbance estimate gradually stabilizes, which proves that the designed finite time disturbance observers are stable in a finite time. It can be seen from Figure 5a that with the stability of the observation system, the tracking performance of the system continues to improve, which shows the effectiveness of the disturbance compensation control law in dealing with uncertain disturbances.

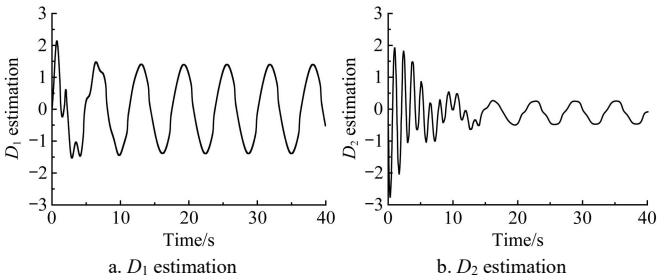

a. D_1 estimation b. D_2 estimation

Figure 5 Disturbance estimation D_1, D_2 of the NRCDC controller

4.3 Implementation of a self-propelled boom sprayer

The active suspension system is implemented on a self-propelled with a 12 m long boom (3WP-500, Essen agricultural machinery Changzhou Co., Ltd, Jiangsu, China), the original boom has no suspension, and the boom is directly mounted to the chassis through the lifting mechanism, and the ground excitation is transmitted directly to the boom, the comparison of the improved active boom and the original un suspended boom is shown Figure 6.

a. Original unsuspended boom b. Active boom suspension system

Figure 6 Comparison of the designed active boom and the original un-suspended boom

The designed active suspension consists of a self-developed controller based on a DSP chip (28377D, Texas Instruments, USA), a proportional valve (MA-QVKZO, VTOZ, China), a hydraulic cylinder, and two ultrasonic sensors (U-GAGE U45Q, Banner, USA) and other components, which is shown in Figure 7. Ultrasonic sensors on both sides of the boom detect the height of both ends of the boom and control the movement of the boom in real-time through the actuator, aligning the boom with the undulations of the ground.

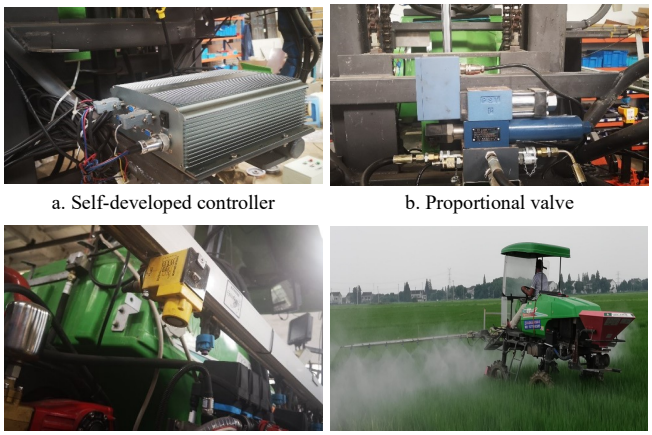

a. Self-developed controller b. Proportional valve

c. Ultrasonic sensor d. Paddy field test site

Figure 7 Implementation and field trials of active suspension system

A comparative test of different control strategies was carried out in a paddy field as shown in Figure 7d. The experimental field is located in the modern agricultural industry demonstration park in Wujiang District, Suzhou City, Jiangsu Province, China. The test time was August 10, 2021. The self-propelled boom sprayer was used to spray pesticides in the test area. The rut depth was about 20 cm, the water depth was 10-15 cm, and the average height of the rice was about 60 cm. The soil nature is paddy soil formed by long-term rice-wheat rotation, the soil irrigation conditions are good, the management level is the same, the soil type is loamy clay, and the characteristics of high viscosity and high water content. Soil compaction data were measured using a soil compaction meter (FieldScout SC 900, Spectrum Technologies, Inc.), In the soil layer between 0-10 cm, the overall soil compactness remained at a low level and changed slowly, with average soil compaction of 310.26 kPa. In the soil layer between 10-20 cm, the soil compaction degree gradually increased, and the increase gradually increased, and the average soil compaction degree was 482.11 kPa.

The sprayer travels at a speed of 4 km/h, rolling angle of the boom and chassis were measured by an inertial measurement system (Ellipse-D-G4A2B1, SBG System, France), whose accuracy of roll angle is 0.05°. Compare the boom angle with the chassis angle as shown in Figure 8. Table 3 lists the comparison of performance evaluation indexes of NRCDC and the other 3 controllers in the field test. The deformation of the soil will cause the chassis of the sprayer to shake violently, and the maximum rolling angle of the chassis is 5.36°. When using the NRCDC controller, all the indexes used to evaluate the boom roll movement are better than the other controllers, and the boom roll angle fluctuates in a small range, with a maximum value of only 1.246°. The test results show that the proposed NRCDC controller can significantly improve the control accuracy of the boom movement and suppress the disturbance caused by the chassis movement. The vibration isolation performance of the pendulum active suspension system designed in this paper also exceeds that of the original unsuspended boom system.

Then the spray deposition distribution of the boom was tested under field conditions. In the field, 6 pieces of water-sensitive papers were arranged for each group of experiments to collect spray deposits of the boom. The water-sensitive papers were placed both on the left and right sides of the sprayer, 2 m, 3 m, and 4 m away from the center of the boom, then the sprayer passed over the water sensitive paper at a speed of 4 km/h.

Five sets of tests were carried out under paddy field conditions, and the sprayed WSPs have been stored in individually marked envelopes and processed in the laboratory by an image analysis system using the image pixel method to obtain coverage on each piece of water-sensitive paper, and then we calculate the coefficient of variation of droplet coverage for five groups of tests, and the comparison of the WSP sampling results (before and after the installation of the active suspension) is listed in Table 4. Compared with the original non-suspension boom, the results of five tests show that the distribution uniformity of the boom is greatly improved after the active suspension is installed.

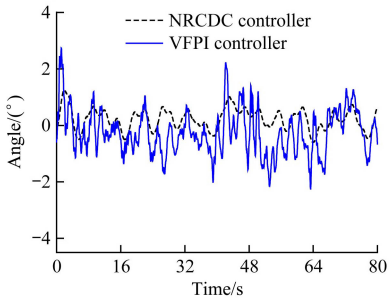

Figure 8 Comparison of the roll angle of boom and chassis in field test

Table 3 Performance indexes of four controllers in field test

Indices	M_e/(°)	μ/(°)	σ/(°)
NRCDC	1.246	0.397	0.293
VFPI	2.739	0.672	0.497
FLC	2.234	0.4884	0.378
RFC	3.933	0.758	0.613

Note: M_e, μ and σ represent the maximum, average and standard deviation of the absolute value of the error, respectively.

Table 4 Comparison of the spray distribution of the original boom and the boom after active suspension installation

Spray distribution		Left Boom			Right boom		
Original unsuspended boom system	Distance/m	2.0[a]	3.0	4.0	2.0	3.0	4.0
	Coverage ratio/%	17.26	24.46	17.32	25.51	36.02	46.97
	CV/%	21.13[b]	41.39	56.73	23.14	41.68	52.79
Active boom suspension system	Coverage ratio/%	25.82	33.36	31.12	27.08	31.04	39.87
	CV/%	15.65	24.68	31.54	13.27	20.52	23.13

Note: [a] The transverse distance measured from the center of the boom. [b] CV of five group test runs.

5 Conclusions

A robust control strategy with disturbance compensation has been proposed for the active pendulum boom suspension in this paper, it integrates a robust controller and disturbance observers through the backstepping method.

To verify the effectiveness of the proposed NRCDC controller, an electro-hydraulic suspension experiment bench with a 28 m long spray boom is established, and a six-degree freedom motion platform is used to generate external disturbance. Comparative experiments with traditional controllers such as FLC, RFC, and VFPI are presented, and the experimental results show that the steady-state tracking error of the proposed NRCDC controller is reduced by 38.81% compared with the FLC controller, reduced by 53.15% compared with the VFPI controller. The tracking performance of the pendulum electro-hydraulic suspension system under disturbance is improved.

Finally, the proposed nonlinear robust control strategy for the active boom system is implemented on a self-propelled sprayer with a boom 12 m in length. The field test results show that all the performance indicators of the NRCDC controller are better than the commonly used controllers. Laboratory and field test results show that the controller can significantly improve the tracking accuracy of the active boom suspension system and can suppress external disturbances.

Nomenclature

Symbol/Unit	Meaning
x_L/m	Displacement of the piston rod of the hydraulic cylinder
β/(°)	The angle between boom and target position
ϑ/(°)	The angle from which the pendulum rod OP deviates from the initial position
ζ/(°)	The angle between rod PQ and rod PR
I_1/kg·m^2	Moment of inertia of the spray boom
K_1/N·m·rad^{-1}	Rotational stiffness coefficient of the suspension around point P
C_1/N·m·s·rad^{-1}	Rotational damping coefficient of the suspension around point P
A_f/N·m	Amplitude of approximate Coulomb friction
f/N·m	Sum of unmodeled dynamics and external disturbances
A_1, A_2/m^2	Effective areas of the two chambers of the hydraulic cylinder
P_1, P_2/Pa	Oil pressure of two chambers
Q_1, Q_2/m^3·s^{-1}	Flow from the servo valve to the two chambers of the hydraulic cylinder
q_1, q_2/m^3·s^{-1}	Lumped modeling errors in the dynamics
β_{e1}, β_{e2}/Pa	The bulk modulus of the hydraulic oil in the left and right chambers of the hydraulic cylinder
P_s, P_r/Pa	Supply pressure and return pressure

$\boldsymbol{\theta}$	Set of unknown parameters in the suspension system
$D_1(x, t)$ $D_2(x, t)$	Mismatched concentrated disturbance and matched concentrated disturbance
u/V	Control input voltage
NRCDC	Non-linear robust controller with disturbance compensation
FLC	Feedback linearization controller
RFC	Direct robust feedback controller
VFPI	Velocity feed-forward proportional-integral controller

Acknowledgements

This work was supported by the National Key Research and Development Program of China (Grant No. 2022YFD2000700), Fundamental Research Funds for Central Research Institutes of China (Grant No. Y2022XK31), R&D projects in key areas of Guangdong Province (Grant No. 2019B0202221001), Jiangsu Modern Agricultural Machinery Equipment and Technology Demonstration and Promotion Project (Grant No. NJ2022-01).

[References]

[1] Carvalho F P. Pesticides, environment, and food safety. Food and Energy Security, 2017; 6(2): 48–60.

[2] Duro J A, Lauk C, Kastner T, Erb K H, Haberl H. Global inequalities in food consumption, cropland demand and land-use efficiency: A decomposition analysis. Global Environmental Change, 2020; 64(7): 23–31.

[3] Jia W, Zhang J, Yan M. Current situation and development trend of boom sprayer. Journal of Chinese Agricultural Mechanization, 2013; 34(4): 19–22. (in Chinese)

[4] He X. Research progress and developmental recommendations on precision spraying technology and equipment in China. Smart Agriculture, 2020; 2(1): 133–146.

[5] Lardoux Y, Sinfort C, Enfält P, Sevila F. Test method for boom suspension influence on spray distribution, Part I: Experimental study of pesticide application under a moving boom. Biosystems Engineering, 2007; 96(1): 29–39.

[6] Lechenet M, Dessaint F P G, Makowski D, Munier-Jolain N. Reducing pesticide use while preserving crop productivity and profitability on arable farms. Nature Plants, 2017; 3(3): 1–6.

[7] Mangus D L, Sharda A, Engelhardt A, Flippo D, Strasser R, Luck J D, et al. Analyzing the nozzle spray fan pattern of an agricultural sprayer using pulse width modulation technology to generate an on-ground coverage map. Transactions of the ASABE, 2017; 60(2): 315–325.

[8] Clijmans L, Swevers J, De Baerdemaeker J, Ramon H. Sprayer boom motion, Part 1: derivation of the mathematical model using experimental system identification theory. Journal of Agricultural Engineering Research, 2000; 76(1): 61–69.

[9] Ramon H, Ba Erdemaeker J D. Spray boom motions and spray distribution: Part 1, Derivation of a mathematical relation. Journal of Agricultural Engineering Research, 1997; 66(1): 23–29.

[10] Jeon H Y, Womac A R, Gunn J. Sprayer boom dynamic effects on application uniformity. Transactions of the ASAE, 2004; 47(3): 647–659.

[11] Herbst A, Osteroth H J, Stendel H. A novel method for testing automatic systems for controlling the spray boom height. Biosystems Engineering, 2018; 174: 115–125.

[12] Anthonis J, Ramon H. Design of an active suspension to suppress the horizontal vibrations of a spray boom. Journal of Sound and Vibration, 2003; 266(3): 573–583.

[13] Anthonis J, Ramon H. SVD H^{∞} controller design for an active horizontal spray boom suspension. Proc. 7th Mediterranean Conf. on Control and Automation, 1999: pp.90–102.

[14] Anthonis J, Audenaert J, Ramon H. Design optimization for the vertical suspension of a crop sprayer boom. Biosystems Engineering, 2005; 90(2): 153–160.

[15] Frost A R, O'Sullivan J A. Verification and use of a mathematical model of an active twin link boom suspension. Journal of Agricultural Engineering Research, 1988; 40(4): 259–274.

[16] Višacki V V, Sedlar A D, Gil E, Bugarin R M, Turan J J, Janic T V, et al. Effects of sprayer boom height and operating pressure on the spray uniformity and distribution model development. Applied Engineering in Agriculture, 2016; 32(3): 341–346.

[17] Balsari P, Gil E, Marucco P, van de Zande J C, Nuyttens D, Herbst A, Gallart M. Field-crop-sprayer potential drift measured using test bench: Effects of boom height and nozzle type. Biosystems Engineering, 2017; 154: 3–13.

[18] Cui L F, Mao H P, Xue X Y. Hydraulic-drive roll movement control of a spray boom using adaptive robust control strategy. Advances in Mechanical Engineering, 2019; 11(2): 1–14.

[19] Cui L F, Xue X Y, Ding S M, Le F X. Development of a DSP-based electronic control system for the active spray boom suspension. Computers and Electronics in Agriculture, 2019; 166: 1–12.

[20] Deprez K, Anthonis J, Ramon H. System for vertical boom corrections on hilly fields. Journal of Sound and Vibration, 2003; 266(3): 613–624.

[21] Anthonis J, Ramon H. Design of an active suspension to suppress the horizontal vibrations of a spray boom. Journal of Sound and Vibration, 2003; 266(3): 573–583.

[22] Gohari M, Tahmasebi M. Active off-road seat suspension system using intelligent active force control. Journal of Low Frequency Noise, Vibration and Active Control, 2015; 34(4): 475–489.

[23] Lu Z, Li S, Wang X. A tracking control of plant spray boom system with semi-active suspension. In 2019 IEEE 3rd Information Technology, Networking, Electronic and Automation Control Conference, 2019; pp.1755–1759.

[24] Yao J, Deng W. Active disturbance rejection adaptive control of hydraulic servo systems. IEEE Transactions on Industrial Electronics, 2017; 64(10): 8023–8032.

[25] Yao B, Tomizuka M. Adaptive robust control of SISO nonlinear systems in a semi-strict feedback form. Automatica, 1997; 33(5): 893–900.

[26] Yao J, Jiao Z, Ma D. Extended-state-observer-based output feedback nonlinear robust control of hydraulic systems with backstepping. IEEE Transactions on Industrial Electronics, 2014; 61(11): 6285–6293.

[27] Guo Q, Zhang Y, Celler B G, Su S W. Backstepping control of electro-hydraulic system based on extended-state-observer with plant dynamics largely unknown. IEEE Transactions on Industrial Electronics, 2016; 63(11): 6909–6920.

[28] Deng W, Yao J. Extended-state-observer-based adaptive control of electro-hydraulic servomechanisms without velocity measurement. IEEE/ASME Transactions on Mechatronics, 2019; 25(3): 1151–1161.

[29] Tahmasebi M, Mailah M, Gohari M, Abd Rahman R. Vibration suppression of sprayer boom structure using active torque control and iterative learning. Part I: Modeling and control via simulation. Journal of Vibration and Control, 2018; 24(20): 4689–4699.

[30] Tahmasebi M, Gohari M, Mailah M, Abd Rahman R. Vibration suppression of sprayer boom structure using active torque control and iterative learning. Part II: Experimental implementation. Journal of Vibration and Control, 2018; 24(20): 4740–4750.

[31] Xue T, Li W, Du Y F, Mao E R, Wen H J. Adaptive fuzzy sliding mode control of spray boom active suspension for large high-clearance sprayer. Transactions of the CSAE, 2018; 34(21): 47–56.

[32] Shtessel Y B, Shkolnikov I A, Levant A. Smooth second-order sliding modes: Missile guidance application. Automatica, 2007; 43(8): 1470–1476.

[33] Khan I, Bhatti A I, Arshad A, Khan Q. Robustness and performance parameterization of smooth second-order sliding mode control. International Journal of Control, Automation and Systems, 2016; 14(3): 681–690.

[34] Ren B, Zhong Q C, Dai J. Asymptotic reference tracking and disturbance rejection of UDE-based robust control. IEEE Transactions on Industrial Electronics, 2016; 64(4): 3166–3176.

[35] Manring N D, Fales R C. Hydraulic control systems. John Wiley & Sons, 2019; pp146–153.

[36] Xu Z, Ma D, Yao J, Ullah N. Feedback nonlinear robust control for hydraulic system with disturbance compensation. Proceedings of the Institution of Mechanical Engineers, Part I. Journal of Systems and Control Engineering, 2016; 230(9): 978–987.

[37] Ma R, Zhao J. Backstepping design for global stabilization of switched nonlinear systems in lower triangular form under arbitrary switchings. Automatica, 2010; 46(11): 1819–1823.

[38] Tao G. A simple alternative to the Barbalat lemma. IEEE Transactions on Automatic Control, 1997; 42(5): 698–701.